liferation may eliminate undesired cells in the donor cell population. Similar cell culture strategies may be used to extend this approach to other somatic precursor cells.

The availability of human ES cells and the possibility of generating autologous ES cells by nuclear transfer provide exciting perspectives for the treatment of human diseases. The efficient generation of ES cell–derived glial cells and their use in a neonatal myelin disease model indicates that this strategy might eventually be applicable to human neurological disorders. Although cell replacement in adult inflammatory myelin diseases such as multiple sclerosis poses additional problems, further optimization of the donor ES cells such as targeted inactivation of disease-related genes or overexpression of factors promoting cell migration and survival may help to meet these challenges.

References and Notes

1. M. J. Evans and M. H. Kaufman, *Nature* **292**, 154 (1981); G. R. Martin, *Proc. Natl. Acad. Sci. U.S.A.* **78**, 7634 (1981).
2. J. A. Thomson *et al.*, *Science* **282**, 1145 (1998); M. J. Shamblott *et al.*, *Proc. Natl. Acad. Sci U.S.A.* **95**, 13726 (1998).
3. I. Wilmut, A. E. Schnieke, J. McWhir, A. J. Kind, K. H. S. Campbell, *Nature* **385**, 810 (1997); T. Wakayama, A. C. Perry, M. Zuccotti, K. R. Johnson, R. Yanagimachi, *ibid.* **394**, 369 (1998).
4. G. Keller, *Curr. Opin. Cell Biol.* **7**, 862 (1995); G. Bain, D. Kitchens, M. Yao, J. E. Huettner, D. I. Gottlieb, *Dev. Biol.* **168**, 342 (1995); A. Fraichard *et al.*, *J. Cell Sci.* **108**, 3181 (1995); M. F. A. Finley, N. Kulkarni, J. E. Huettner, *J. Neurosci.* **16**, 1056 (1996); M. Li, L. Pevny, R. Lovell-Badge, A. Smith, *Curr. Biol.* **8**, 971 (1998).
5. R. McKay, *Science* **276**, 66 (1997); O. Bögler, D. Wren, S. C. Barnett, H. Land, M. Noble, *Proc. Natl. Acad. Sci. U.S.A.* **87**, 6368 (1990).
6. A. K. Groves *et al.*, *Nature* **362**, 453 (1993); W. F. Blakemore, N. J. Olby, R. J. M. Franklin, *Brain Pathol.* **5**, 443 (1995); F. Lachapelle, *ibid.*, p. 289; I. D. Duncan, W. E. Grever, S. C. Zhang, *Mol. Med. Today* **3**, 554 (1997).
7. ES cells [line J1 (*21*), passage number ≤ 17] were grown on γ-irradiated embryonic fibroblasts in Dulbecco's modified Eagle's medium (DMEM) containing 20% fetal bovine serum, 0.1 mM 2-mercaptoethanol, nucleosides, nonessential amino acids, and human recombinant leukemia inhibitory factor (LIF, Life Technologies; 1000 units/ml). Cells were passaged once onto gelatin-coated dishes and then aggregated to form embryoid bodies in the absence of LIF. We plated 4-day-old embryoid bodies in tissue culture dishes and propagated them for 5 days in ITSFn medium [DMEM/F12 supplemented with 5 μg/ml insulin, 50 μg/ml transferrin, 30 nM selenium chloride, and 5 μg/ml fibronectin (*8*)]. Cells were then trypsinized, plated in polyornithine-coated dishes (15 μg/ml), and propagated in DMEM/F12 supplemented with insulin (25 μg/ml), transferrin (50 μg/ml), progesterone (20 nM), putrescine (100 μM), selenium chloride (30 nM) plus FGF2 (10 ng/ml), and laminin (1 μg/ml). After 5 days, cells were harvested by scraping in calcium- and magnesium-free Hanks' buffered salt solution (CMF-HBSS), triturated to a single-cell suspension, replated at a 1:5 ratio, and grown to subconfluency in the presence of FGF2 (10 ng/ml) and EGF (20 ng/ml). Cells were then passaged at a 1:5 ratio and again grown to subconfluency in the presence of FGF2 (10 ng/ml) and PDGF-AA (10 ng/ml). Human recombinant FGF2, EGF, and PDGF-AA (R&D Systems, Minneapolis, MN) were added daily and the medium was replaced every 2 days. In vitro differentiation was induced by growth factor withdrawal.
8. S. Okabe, K. Forsberg-Nilsson, A. C. Spiro, M. Segal, R. D. G. McKay, *Mech. Dev.* **59**, 89 (1996).
9. M. C. Raff, R. H. Miller, M. Noble, *Nature* **303**, 390 (1983).
10. Astrocytic and oligodendroglial differentiation were assessed by immunofluorescence analysis using antibodies to A2B5 (Boehringer; 1:200), O4 (Boehringer; 1:5) and GFAP (ICN; 1:100). Similar results were obtained using the ES cell line CJ7 (*22*) (passage number ≤ 18). Four days after growth factor withdrawal, 31.4 ± 3.6% and 35.0 ± 7.4% of the cells were immunoreactive to the O4 and GFAP antibodies, respectively (*n* = 5).
11. I. Sommer and M. Schachner, *Dev. Biol.* **83**, 311 (1981).
12. O. Brüstle and K. Karram, data not shown.
13. Cells growing in medium containing FGF2 and PDGF were harvested and triturated to a single-cell suspension. Spinal cord transplants were performed as described (*23*). Following laminectomy at the thoracolumbar transition, 100,000 cells in a volume of 1 μl CMF-HBSS were injected into the dorsal column of 7-day-old rnd rats at one or several levels. The recipient animals received daily i.p. injections of cyclosporin (10 mg/kg body weight). All procedures were done in accordance with institutional guidelines.
14. M. E. Hodes, V. M. Pratt, S. R. Dlouhy, *Dev. Neurosci.* **15**, 383 (1993).
15. Transplant recipients were perfusion-fixed with 4% paraformaldehyde at 3 weeks of age. Brains and spinal cords were processed for vibratome sectioning. Selected spinal cord transplant recipients were processed for semi- and ultrathin sectioning by routine procedures. Primary antibodies used for immunohistochemistry were anti-PLP (1:500), anti-MBP (Boehringer; 1:200), anti-CNP (Sigma; 1:200), and anti-GFAP (ICN; 1:100). Antigens were visualized using appropriate peroxidase-conjugated secondary antibodies. Identification of donor cells by DNA in situ hybridization with a probe to mouse satellite DNA was done as described (*16*).
16. O. Brüstle, U. Maskos, R. D. G. McKay, *Neuron* **15**, 1275 (1995); O. Brüstle *et al.*, *Nature Biotechnol.* **16**, 1040 (1998).
17. G. Fishell, *Development* **121**, 803 (1995); K. Campbell, M. Olsson, A. Björklund, *Neuron* **15**, 1259 (1995).
18. For intracerebral transplantation, 2 × 10⁵ to 9 × 10⁵ cells in a volume of 4 to 9 μl were injected into the ventricle of E17 rat embryos as described (*16*).
19. A. G. Smith *et al.*, *Nature* **336**, 688 (1988).
20. O. Brüstle *et al.*, *Proc. Natl. Acad. Sci. U.S.A.* **94**, 14809 (1997); J. Dinsmore *et al.*, *Cell Transplant.* **5**, 131 (1996); T. Deacon, J. Dinsmore, L. C. Costantini, J. Ratliff, O. Isacson, *Exp. Neurol.* **149**, 28 (1998).
21. E. Li, T. H. Bestor, R. Jaenisch, *Cell* **69**, 915 (1992).
22. P. J. Swiatek and T. Gridley, *Genes Dev.* **7**, 2071 (1993).
23. J. P. Hammang, D. R. Archer, I. D. Duncan, *Exp. Neurol.* **147**, 84 (1997).
24. We thank I. Griffiths for the PLP antibody and R. Buschwald for excellent technical assistance. This work was supported by a Junior Research Award from the state of Nordrhein-Westfalen (O.B.), the BONFOR program (O.B.), and NIH grant NS33710 (I.D.D.).

Two-Metal-Ion Catalysis in Adenylyl Cyclase

John J. G. Tesmer,[1] Roger K. Sunahara,[2] Roger A. Johnson,[3] Gilles Gosselin,[4] Alfred G. Gilman,[2] Stephen R. Sprang[1]*

Adenylyl cyclase (AC) converts adenosine triphosphate (ATP) to cyclic adenosine monophosphate, a ubiquitous second messenger that regulates many cellular functions. Recent structural studies have revealed much about the structure and function of mammalian AC but have not fully defined its active site or catalytic mechanism. Four crystal structures were determined of the catalytic domains of AC in complex with two different ATP analogs and various divalent metal ions. These structures provide a model for the enzyme-substrate complex and conclusively demonstrate that two metal ions bind in the active site. The similarity of the active site of AC to those of DNA polymerases suggests that the enzymes catalyze phosphoryl transfer by the same two-metal-ion mechanism and likely have evolved from a common ancestor.

Mammalian ACs are integral membrane proteins that catalyze the synthesis of the second messenger adenosine 3′,5′-monophosphate (cAMP) from ATP. Many signaling path-

[1]Howard Hughes Medical Institute, Department of Biochemistry, University of Texas Southwestern Medical Center, 5323 Harry Hines Boulevard, Dallas, TX 75235–9050, USA. [2]Department of Pharmacology, University of Texas Southwestern Medical Center, 5323 Harry Hines Boulevard, Dallas, TX 75235–9041, USA. [3]Department of Physiology and Biophysics, Health Sciences Center, State University of New York, Stony Brook, NY 11794–8661, USA. [4]UMR CNRS-USTL 5625, Laboratoire de Chimie Bioorganique, Sciences et Techniques du Languedoc, Université Montpellier II, 34095 Montpellier, Cedex 5, France.

*To whom correspondence should be addressed. E-mail: sprang@howie.swmed.edu

ways converge on and regulate the enzyme (*1*), including those of heterotrimeric GTP-binding proteins (G proteins), which couple the activation of heptahelical receptors on the cell surface to subsequent changes in AC activity. G proteins bind directly to the catalytic core of AC, which consists of two homologous cytoplasmic domains, C_{1a} and C_{2a}. These domains can be expressed as independent polypeptides in *Escherichia coli* and, when mixed, form a heterodimer that exhibits catalytic activity as well as sensitivity to $G_s\alpha$ and $G_i\alpha$, the stimulatory and inhibitory G protein α subunits (*2–4*).

We recently determined the crystal structure of a complex between $G_s\alpha$ and the C_{1a}: C_{2a} heterodimer (Fig. 1A) and proposed a

mechanism for AC activation by the α subunit (5). By soaking crystals of the complex with the inhibitor 2′-deoxy-3′-AMP · pyrophosphate (2′-d-3′-AMP · PP$_i$), we also located the active site of AC (Fig. 1B). Upon binding, the inhibitor induces the collapse of several conserved loops to form the active site of the enzyme. Modeling studies predict that the binding of ATP elicits a similar conformational change from "open" to "closed." However, a catalytic mechanism for the synthesis of cAMP was not obvious from the 2′-d-3′-AMP · PP$_i$–inhibited structure. In particular, the active site lacked either an obvious catalytic base, which would abstract a proton from the 3′ hydroxyl of ATP, or a second metal ion, which would be con-

sistent with both kinetic models of enzyme activity and recent information obtained from mutagenesis studies (6).

The reaction catalyzed by AC is similar to those of DNA polymerases. Both enzymes catalyze the attack of the 3′ hydroxyl of ribose on the α phosphate of a nucleoside triphosphate. Despite no obvious sequence homology, the enzymes do possess similar domains (7). Of the four known families of DNA polymerases, three have a core "palm" domain composed of a βαββαβ motif. At distinct topological locations within this motif are two invariant aspartic acid residues that coordinate two catalytic metal ions (8–10). The C$_{1a}$ and C$_{2a}$ domains of AC also contain a βαββαβ motif, but only C$_{1a}$ bears

the analogous aspartic acids. If AC is indeed related to DNA polymerases (7) and if its reaction is catalyzed by the same mechanism, then two catalytic metal ions are also expected to bind to the C$_{1a}$ domain of AC. Mutation of the two aspartic acids in C$_{1a}$ should be as catalytically devastating as the analogous mutations in DNA polymerases (11).

To define the active site of AC unambiguously, we determined structures of AC in complex with the competitive substrate analogs: β-L-2′,3′-dideoxyadenosine 5′-triphosphate (β-L-2′,3′-dd-5′-ATP), which has a median inhibitory concentration (IC$_{50}$) of ~24 nM with native enzyme from rat brain (12), and adenosine 5′-(α-thio)-triphosphate (R$_p$) (ATPαS-R$_p$), which has an IC$_{50}$ of 1 μM

Fig. 1. Complexes of ATP analog inhibitors with the catalytic core of AC (31). (**A**) The C$_{1a}$:C$_{2a}$ catalytic core of AC viewed along its pseudo-twofold axis toward what is believed to be the cytoplasmic face of the molecule. Forskolin (FSK) and ATP, which bind between the C$_{1a}$ (tan) and C$_{2a}$ (mauve) domains, are shown as stick models. The switch II helix of G$_s$α, which forms much of the interface with AC, is depicted as a red rod. (**B**) Model of ATP bound in the active site. The side chain of N1025 is modeled after its conformation in the AC · ATPαS-R$_p$ · Mn structure (Fig. 1D), whereas all other elements are those of the AC · βLddATP · Mn structure (Fig. 1C). Thin black lines depict the coordination of the metal ions. The fifth ligand to metal A is a carboxylate oxygen from D440 and is obscured in this view. Protein and inhibitor residues are drawn as stick models, metals as magenta metallic spheres, and water molecules as red spheres. Carbon atoms are gray, nitrogens blue, oxygens red, phosphorous green, and sulfur yellow. Amino acids labeled according to their position in canine type V AC for C$_{1a}$ and rat type II AC for C$_{2a}$. (**C**) The left panel portrays the active site of the AC · βLddATP · Mn complex. Secondary structure is labeled as previously defined (5). Superimposed is electron density from a 2.8 Å resolution |F$_{O_{Mg}}$| − |F$_c$| omit map (blue wire cage) contoured at 2.5σ. Structural elements donated by the C$_{1a}$ and C$_{2a}$ domains of AC are shown in tan and mauve, respectively. The right panel is a closeup of the triphosphate of the inhibitor. For clarity, the image has been rotated slightly from the view in the left panel. The green and purple wire cages represent electron density contoured at 5σ for 3.0 Å |F$_{O_{Zn}}$| − |F$_{O_{Mg}}$| and 2.8 Å |F$_{O_{Mn}}$| − |F$_{O_{Mg}}$| omit maps, respectively, demonstrating that Zn^{2+} preferentially binds at site A and Mn^{2+} at site B. The peak height is 8.2σ for the Zn^{2+} electron density and 11.3σ for Mn^{2+}. |F$_{O_{Mg}}$|, |F$_{O_{Mn}}$|, and |F$_{O_{Zn}}$| are the observed structure factor amplitudes of the AC · βLddATP · Mg, AC · βLddATP · Mn, and AC · βLddATP · Zn data sets, respectively. (**D**) The active site of AC · ATPαS-R$_p$ · Mn (left) and a closeup view of its thiotriphosphate (right). Superimposed is electron density from a 3.0 Å |F$_o$| − |F$_c$| omit map contoured at 2.5σ. A 7σ peak marks the position of metal B and is modeled as Mn^{2+}. A 2σ peak marks the position of metal A and is modeled as Mg^{2+}, although it could also be a weakly bound Mn^{2+}.
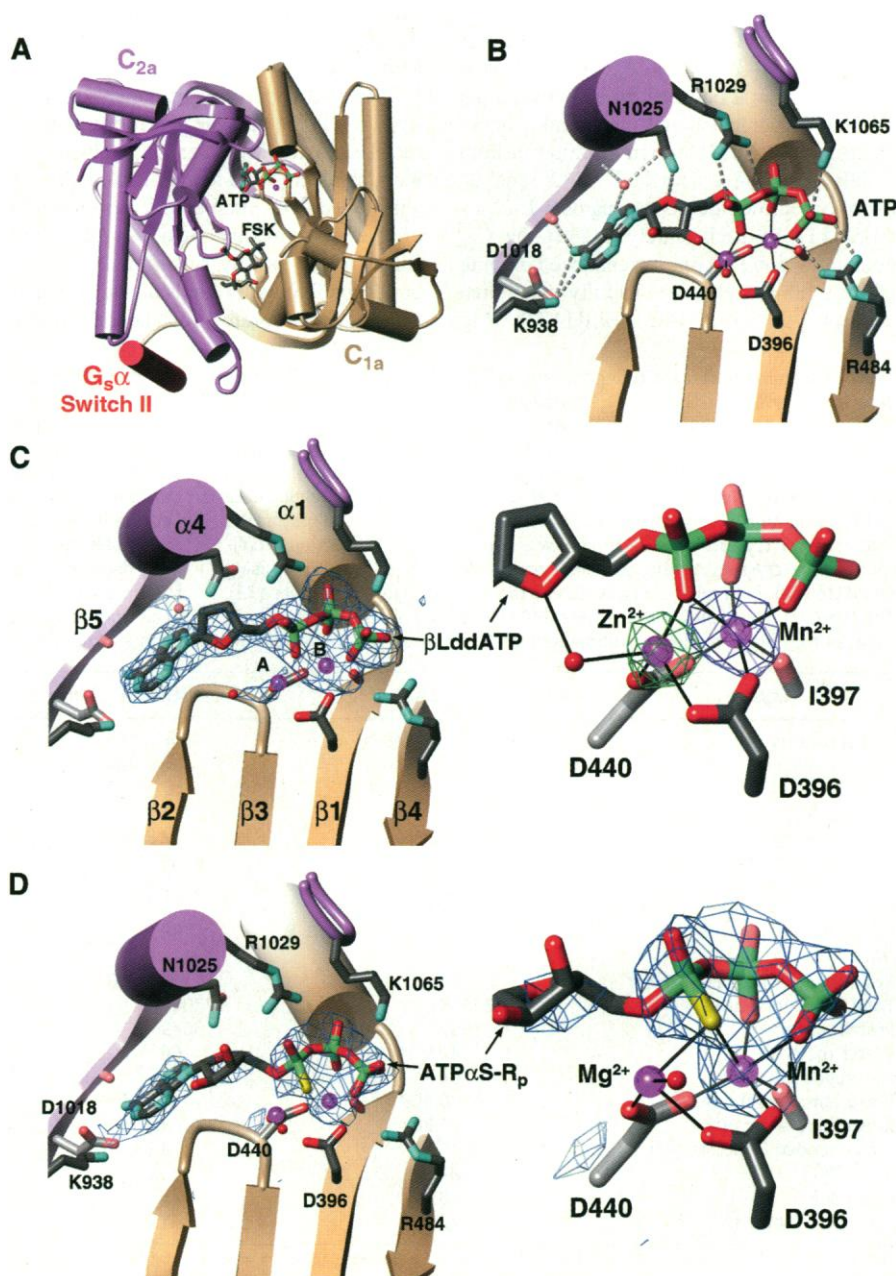
with the soluble AC used in these crystallographic studies (13, 14). Crystals of the $G_s\alpha$: C_{1a}:C_{2a} complex were soaked with various combinations of ATP analogs and metal ions (15). Four structures were ultimately determined: $G_s\alpha$:C_{1a}:C_{2a} · β-L-2′,3′-dd-5′-ATP · 2Mg^{2+} (AC · βLddATP · Mg), $G_s\alpha$:C_{1a}:C_{2a} · β-L-2′,3′-dd-5′-ATP · Mg^{2+} · Mn^{2+} (AC · βLddATP · Mn), $G_s\alpha$:C_{1a}:C_{2a} · β-L-2′,3′-dd-5′-ATP · Mg^{2+} · Zn^{2+} (AC · βLddATP · Zn), and $G_s\alpha$:C_{1a}:C_{2a} · ATPαS-R_p · Mg^{2+} · Mn^{2+} (AC · ATPαS-R_p · Mn) (Table 1). In each case, the AC catalytic core was in the closed conformation previously described for the complex of $G_s\alpha$:C_{1a}:C_{2a} with the inhibitor 2′-d-3′-AMP · PP$_i$ (5).

β-L-2′,3′-dd-5′-ATP contains a ribose moiety with opposite absolute configuration of that in ATP. Even so, β-L-2′,3′-dd-5′-ATP occupies the active site in a similar fashion to 2′-d-3′-AMP · PP$_i$, with the purine ring binding in a pocket formed between the C_{1a} and C_{2a} domains and the β and γ phosphates binding the P loop in a similar fashion as PP$_i$ (Fig. 1C). The lack of 2′ and 3′ hydroxyls allows the ribose ring of β-L-2′,3′-dd-5′-ATP to pack snugly against the C_{2a} domain, which explains the enhanced binding of this inhibitor relative to its fully substituted analogs (12). In the AC · βLddATP · Mg

structure, β-L-2′,3′-dd-5′-ATP appears to bind as a complex with two metal ions. The first metal (metal A) is coordinated by the pro-R oxygen of the α phosphate, a carboxylate oxygen from each of the invariant aspartic acid residues [Asp^{396} (D396) and D440], and a water molecule. The four ligands form a tetrahedral coordination sphere. The second metal (metal B) was previously observed in the 2′-d-3′-AMP · PP$_i$ complex with $G_s\alpha$:C_{1a}:C_{2a} and is octahedrally coordinated by one oxygen from each aspartic acid; an unesterified oxygen from each of the α, β, and γ phosphates; and the backbone carbonyl of Ile^{397}. Addition of Zn^{2+} to generate AC · βLddATP · Zn, or of Mn^{2+} to generate AC · βLddATP · Mn, increases the electron density at the A or B sites, respectively (Fig. 1C). These data conclusively demonstrate that there are two metal ion binding sites in the active site of AC.

Although both are presumably occupied by Mg^{2+} in the cell, the specificity of the two metal sites for Mn^{2+} or Zn^{2+}, which have identical charge and similar ionic radii, probably reflects the number and stereochemistry of the coordinating ligands. Accordingly, Zn^{2+}, which readily accommodates four ligands, preferentially binds at site A, whereas Mn^{2+}, which prefers octahedral coordina-

tion, binds at site B. Mn^{2+} is an activator of AC, whereas Zn^{2+} is an inhibitor [IC_{50} = 15 μM (13)]. Although Zn^{2+} does not generally inhibit two-metal-ion–utilizing enzymes (16–18), it does inhibit several DNA and RNA polymerases (19). In these enzymes and AC, Zn^{2+} may perturb the coordination of the reactive groups and thus affect enzyme activity. These changes may not be evident in AC · βLddATP · Zn where there is no 3′ hydroxyl to coordinate metal A.

The structure of the AC · ATPαS-R_p · Mn complex rationalizes the potent inhibitory properties that result from substitution of a thiol group for the R_p α phosphate oxygen and reveals additional features that likely exist in the active site of an AC · ATP complex. Two metal ions are also apparent in the structure of this complex (Fig. 1D). The coordinating ligands for metal B are the same as in the AC · βLddATP structures, except that a sulfur is substituted for the pro-R oxygen on the α phosphate. Metal A has only four obvious ligands: the sulfur atom of ATPαS-R_p, one oxygen from each aspartic acid, and a water molecule positioned transaxial to the oxygen ligand donated by D440. There are probably additional water ligands that are not apparent because of disorder or the resolution of the experiment. The thiotriphosphate of

Table 1. Summary of data collection and refinement statistics. Diffraction data from crystals of $G_s\alpha$:C_{1a}:C_{2a} complexes were measured on a 2k × 2k ADSC Quantum 4 charge-coupled device area detector using 0.923 Å radiation from the F1 beam line at the Cornell High Energy Synchrotron Source (CHESS). All crystals were flash-frozen in nitrogen-cooled liquid propane on 0.1 to 0.2-mm cryoloops (Hampton) and were maintained throughout data collection in an MSC cryostream at −180°C. With a 0.1-mm collimator, the mosaicity for crystals of the complex was typically 0.5°. Diffraction amplitudes from crystals of the complex were indexed and integrated using MOSFLM (32) and scaled using SCALA of the CCP4 programming suite (33). The $G_s\alpha$:C_{1a}:C_{2a} complex with 2′-d-3′-AMP · PP$_i$ (with inhibitor removed) was used as the initial model for refinement of the four structures. After one round of rigid body refinement, Powell minimization, and simulated annealing with CNS (34), the program O (35) was used to fit inhibitors and metal ions into positive difference density in the active site. The models were subsequently refined for multiple rounds in CNS. Anisotropic overall B factors and a bulk solvent mask were used throughout refinement. No residues in any of the four models are found in disallowed regions of the Ramachandran plot. Because the $G_s\alpha$ used in the current study had been treated with trypsin, there are notable differences in $G_s\alpha$ between the structures reported here and previously determined structures of $G_s\alpha$:C_{1a}:C_{2a}. By comparing electron density maps, trypsin appears to cut after R38 of bovine $G_s\alpha$, cleaving the NH$_2$-terminal helix from the protein, and after R389 at the end of α5. The latter cut results in an alternate conformation for the COOH-terminal residues of the protein.

Crystal	AC · βLddATP · Mg	AC · βLddATP · Mn	AC · βLddATP · Zn	AC · ATPαS-R_p · Mr
Cell constants (Å)	a = 118.3	a = 118.2	a = 118.4	a = 118.9
	b = 134.2	b = 134.2	b = 134.2	b = 134.9
	c = 71.4	c = 71.3	c = 71.6	c = 72.2
Crystals (n)	2	1	1	1
D_{min} (Å, along $a*$ and $b*$)	2.8	2.8	3.0	3.0
Unique reflections	22671	28238	21550	20230
Average redundancy	3.8	3.4	3.5	2.6
R_{sym} (%)*	13.6	10.6	13.7	14.2
Completeness (%)	80.2	98.8	92.4	85.6
$\langle I/\sigma_I \rangle$	8.6	12.0	9.8	7.9
Res. range for refinement (Å)†	15 − 2.8	15 − 2.8	15 − 3.0	15 − 3.0
Total reflections used	21963	27082	21017	19678
Protein atoms (n)	5657	5649	5633	5657
Water molecules (n)	42	66	46	34
Heterogen atoms (n)	94	106	107	108
Rmsd bond lengths (Å)	0.008	0.007	0.007	0.008
Rmsd bond angles (°)	1.28	1.25	1.24	1.17
Rmsd bonded B factors (Å^2)	1.7	2.3	1.9	2.1
R_{work} (%)‡	22.2	20.6	20.4	22.0
R_{free} (%)§	28.4	25.2	26.2	26.6
Average B factor (Å^2)	43.1	41.0	35.1	43.2

*$R_{sym} = \Sigma_h\Sigma_i |I(h)-I(h)_i| / \Sigma_h\Sigma_i I(h)_i$, where $I(h)$ is the mean intensity after rejections.   †Due to anisotropy, data with an l index greater than 20 were omitted from refinement.   ‡$R_{work} = \Sigma_h \|F_o(h)| - |F_c(h)\|/\Sigma_h |F_o(h)|$; no I/σ cutoff was used during refinement.   §Ten percent of the complete data set was excluded from refinement to calculate R_{free}.

ATPαS-R$_p$ is well ordered and the sulfur is about 3 Å from each metal ion. It is therefore unclear whether the sulfur serves as a ligand for either metal. Even though each phosphorous atom of ATPαS-R$_p$ resides in a similar position to those of β-L-2′,3′-dd-5′-ATP, the overall conformation of their triphosphate moieties is distinct (compare Fig. 1, C and D). The conformation of the ATPαS thiotriphosphate helps accommodate the bulkier sulfur atom by rotating the α phosphate slightly up from its position in β-L-2′,3′-dd-5′-ATP. However, this results in distorted coordination geometry for both metals. The ribose moiety of the inhibitor is poorly ordered, perhaps because the sulfur atom precludes the 3′ hydroxyl of the inhibitor from binding metal A. The 3′ hydroxyl is not in position for attack on the α phosphate.

An aspargine at position 1025 in type II AC is conserved in all adenylyl and guanylyl cyclases (Fig. 1D). Mutation of this residue in type II AC reduces the catalytic constant 30 to 100 times but does not dramatically affect the Michaelis constant (K_m) for ATP (20). Although several alternative roles have been proposed for this residue (5, 20, 21), the structure of AC · ATPαS-R$_p$ · Mn demonstrates that Asn[1025] forms a hydrogen bond with the O4′ oxygen of ribose. Mutation of this residue could result in misorientation of the substrate in the active site.

We expect the purine and triphosphate moieties of β-L-2′,3′-dd-5′-ATP to resemble closely those of ATP in an enzyme-substrate complex. Although the orientation of the ribose ring of ATP is expected to differ from that of ATPαS-R$_p$ in the AC · ATPαS-R$_p$ · Mn complex, we still expect the O4′ oxygen of ATP to form a hydrogen bond with Asn[1025]. In addition, metal A likely serves as a Lewis acid that enhances the nucleophilicity of the 3′ hydroxyl of ATP. With these constraints, a model for the substrate ATP can be built such that the 3′ hydroxyl of ribose is 2 Å from metal A and is positioned

for in-line attack on the α phosphate (Fig. 1B). The coordination sphere of metal A is roughly square pyramidal in our AC · ATP model complex. The ligands are the 3′ hydroxyl, the pro-R unesterified oxygen of the α phosphate, a carboxylate oxygen from D396 and D440, and a water molecule analogous to that observed in the structure of AC · ATPαS-R$_p$ · Mn (Fig. 1D). Due to close contacts with the 3′ hydroxyl and the C^β atom of Cys[441], it is not clear whether there is room for a second water ligand for metal A as there is in T7 DNA polymerase (T7DNAP) and Thermus aquaticus DNA polymerase I (TAQP) (8, 10).

The structure of the product cAMP, as it is observed in small molecule crystal structures (22), is incompatible with the active site of AC when optimally superimposed on ATP. Its phosphate moiety overlaps with metal A and D440, which may explain why cAMP is preferentially released from the active site before the other product, PP$_i$ (23).

To test the role of the two invariant aspartic acid residues in the active site of AC, each was mutated to alanine and asparagine, alone and in combination, to generate the eight (31) mutants D396A, D396N, D440A, D440N, D396A/D440A, D396N/D440N, D396N/D440A, and D396A/D440N. Residues analogous to D396 and D440 have been previously mutated to alanine in ACs, but not in the system employed for our crystallographic studies and not in the same protein, preventing a meaningful comparison of their effects (21, 24). As was the case for the analogous mutations in T7 RNA polymerase (T7RNAP) and human immunodeficiency virus type I reverse transcriptase (HIVRT), all of the mutations were largely inactivating (11) (Table 2). No activity was observed for any of the double mutants. Activity for each of the single mutants was reduced approximately 2000 times with the physiological metal Mg^{2+} and 200 times with Mn^{2+}. For all the single mutants, K_m was increased 2- to 10-fold. For

both D396 and D440 there is no discernable difference in limiting rate constant (V_{max}) or K_m for ATP between the alanine and asparagine mutants. However, mutations at D440 were only half as detrimental to the K_m than were mutations at D396. Therefore, D396 may play a more important role in binding substrate. D440 is unlikely to be a general base, as suggested previously, because mutation of this residue does not abrogate activity and no more so than mutation of D396.

The remarkable similarity of the βαββαβ fold in AC to those of the palm domains of T7DNAP, HIVRT, and TAQP, as well as the bacteriophage polymerase α homolog gp43, is equally striking at the molecular level (25). The active sites of these enzymes are supported by a platform of four β strands. A P loop following the first of these creates the triphosphate binding site. Two conserved aspartate residues coordinate two metal ions in identical fashion, and the distinct metal preferences of the two sites are the same in AC and T7DNAP (8). Hence, like phosphatases, exonucleases, ribozymes, and polymerases (8, 16, 18, 26), AC employs a two-metal-ion catalytic mechanism. Conservation of both fold and mechanism suggests a common evolutionary origin for the AC and PolI family catalytic domains.

Both DNA polymerases and AC undergo a transition from an open to a closed conformational state upon binding nucleotide substrates (25, 27). In DNA polymerases, the transition involves the collapse of the so-called "fingers" domain on the palm domain. In AC, several loops, including a rudimentary fingers domain, collapse around ATP to form the competent active site. In each enzyme, the collapse brings basic residues into the active site that stabilize the triphosphate of the substrate, the pentavalent phosphate transition state of the reaction, and the pyrophosphate leaving group. For polymerases, the conformational change appears crucial to the fidelity (28) and processivity (29) of the reaction. In AC, active site closure is required to

Table 2. Kinetic parameters for active site mutants of the AC catalytic core. Site-directed mutagenesis of the C$_{1a}$ domain of type V AC was performed using the Quickchange (Stratagene) mutagenesis kit (30). Overlapping antiparallel pairs of mutagenic oligonucleotides encompassing regions of pQE60-H6-VC$_I$ (2) that code for residues D396 or D440 were used. The sequences of the mutagenic oligonucleotides are available by request. Double mutants were generated by successive mutagenesis. All proteins were expressed in E. coli and purified as previously described (2). The purified mutant proteins were capable of protein complex formation with IIC$_2$, G$_s$α · GTPγS, and forskolin as measured by gel filtration chromatography, indicating correct protein folding (13). Adenylyl cyclase activity was measured after activation of the enzyme by G$_s$α · GTPγS. IIC$_2$ (2 μM) was reconstituted with wild-type VC$_I$ (2 nM) or mutant VC$_I$ (20 nM). All assays were performed in the presence of 5 mM (free) Mg^{2+}. Where noted, Mn^{2+} was present at 5 mM. Double mutants have negligible activity, and values for kinetic constants could not be determined.

Mutation*	G$_s$α · GTPγS + Mg^{2+}			G$_s$α · GTPγS + Mn^{2+}		
	K_m (mM)	V_{max} (s^{-1})	V_{max}/K_m (s^{-1} mM)	K_m (mM)	V_{max} (s^{-1})	V_{max}/K_m (s^{-1} mM)
WT†	0.56	15.5	27.7	0.094	8.8	93.0
D396A	4.5	0.074	0.016	0.293	0.044	0.15
D396N	6.9	0.109	0.016	0.285	0.065	0.23
D440A	2.8	0.071	0.025	0.126	0.065	0.51
D440N	1.5	0.079	0.053	0.17	0.068	0.40

*Amino acid numbering is for canine type V AC.   †WT, wild type.

achieve a productive and substrate-specific catalytic complex, and this induced-fit mechanism provides a direct opportunity for allosteric regulation. In analogy to an allosteric dimer, the active site of AC is formed at the interface between dyad-related homologous domains. Thus, AC provides two symmetrically related binding sites for the homologous G proteins $G_s\alpha$ and $G_i\alpha$ (4, 5). We suggest that $G_s\alpha$ facilitates collapse of the active-site loops from C_{1a} and C_{2a} around the substrate ATP to form an competent active site, whereas $G_i\alpha$ hinders such collapse and stabilizes an open, inactive conformation of the enzyme.

References and Notes

1. R. K. Sunahara, C. W. Dessauer, A. G. Gilman, Annu. Rev. Pharmacol. Toxicol. 36, 461 (1996); D. M. F. Cooper, Ed., Advances in Second Messenger and Phosphoprotein Research, vol. 32 (Lippincott-Raven, Philadelphia, PA, 1998).
2. R. K. Sunahara, C. W. Dessauer, R. E. Whisnant, C. Kleuss, A. G. Gilman, J. Biol. Chem. 272, 22265 (1997).
3. R. E. Whisnant, A. G. Gilman, C. W. Dessauer, Proc. Natl. Acad. Sci. U.S.A. 93, 6621 (1996); S.-Z. Yan, D. Hahn, Z.-H. Huang, W.-J. Tang, J. Biol. Chem. 271, 10941 (1996).
4. C. W. Dessauer, J. J. Tesmer, S. R. Sprang, A. G. Gilman, J. Biol. Chem. 273, 25831 (1998).
5. J. J. G. T. Tesmer, R. K. Sunahara, A. G. Gilman, S. R. Sprang, Science 278, 1907 (1997).
6. D. L. Garbers and R. A. Johnson, J. Biol. Chem. 250, 8449 (1975); G. Zimmermann, D. Zhou, R. Taussig, ibid. 273, 19650 (1998).
7. P. J. Artymiuk, A. R. Poirrette, D. W. Rice, P. Willett, Nature 388, 33 (1997).
8. S. Doublié, S. Tabor, A. M. Long, C. C. Richardson, T. Ellenberger, ibid. 391, 251 (1998).
9. H. Huang, R. Chopra, G. L. Verdine, S. C. Harrison, Science 282, 1669 (1998).
10. Y. Li, S. Korolev, G. Waksman, EMBO J. 17, 7514 (1998).
11. N. Kaushik et al., Biochemistry 35, 11536 (1996); A. Y. Woody, S. S. Eaton, P. A. Osumi-Davis, R. W. Woody, ibid., p. 144.
12. I. Shoshani, V. Boudou, C. Pierra, G. Gosselin, R. A. Johnson, unpublished data.
13. R. K. Sunahava and J. J. G. Tesmer, data not shown.
14. F. Eckstein, P. Romaniuk, W. Heideman, D. Storm, J. Biol. Chem. 256, 9118 (1981).
15. The recombinant C_{1a} domain from canine type V AC, the C_{2a} domain from rat type II AC, and bovine $G_{s\alpha}$ were expressed in E. coli and purified as previously described (30). $G_{s\alpha}$ was activated with $Mg^{2+} \cdot GTP\gamma S$ and then subjected to limited proteolysis by trypsin. Crystals of the ternary complex between C_{1a}, C_{2a}, and $G_{s\alpha}$ were grown as previously described (5). All crystals were harvested in cryoprotectant (5) to which was added various combinations of inhibitors and metal ions, described as follows: for $AC \cdot \beta LddATP \cdot Mg$, 5 mM $MgCl_2$ and 380 µM β-L-2',3'-dd-5'-ATP; for $AC \cdot \beta LddATP \cdot Mn$, 250 µM $MgCl_2$, 500 µM $MnCl_2$, and 380 µM β-L-2',3'-dd-5'-ATP; for $AC \cdot \beta LddATP \cdot Zn$, 250 µM $MgCl_2$, 500 µM $ZnCl_2$, and 380 µM β-L-2',3'-dd-5'-ATP; for $AC \cdot ATP\alpha S$-$R_p \cdot Mn$, 500 µM $MgCl_2$, 500 µM $MnCl_2$, and 1 mM ATPαS-R_p. Crystals of $AC \cdot \beta LddATP \cdot Mg$, $AC \cdot \beta LddATP \cdot Mn$, and $AC \cdot \beta LddATP \cdot Zn$ were soaked for 1 to 2 hours; the conformation of AC in these complexes was closed. $AC \cdot ATP\alpha S$-$R_p \cdot Mn$ was soaked for 6 hours to achieve a closed conformation; 2-hour soaks resulted in structures of the open conformation of AC. AC complexes with inhibitors such as $ATP \cdot Zn^{2+}$, ATPαS-$S_p \cdot Zn^{2+}$, and 2'-iodo-ATP $\cdot Mg^{2+}$ also adopt the open conformation, and each metal site exhibits the same preference for either Mn^{2+} or Zn^{2+} as observed in the closed conformation (13). Strong electron density is observed for the β and γ phosphates of these inhibitors in

the presence of Mg^{2+} alone or of Mn^{2+} and Mg^{2+}, and for the entire triphosphate in the presence of Zn^{2+} and Mg^{2+}. Much weaker density corresponding to a purine ring is observed in the purine binding pocket of these complexes. However, the purine and triphosphate densities are not continuous, and a single model of ATP cannot be built to accommodate both purine and triphosphate binding sites.
16. E. E. Kim and H. W. Wyckoff, J. Mol. Biol. 218, 449 (1991).
17. V. Derbyshire, J. K. Pinsonneault, C. M. Joyce, Methods Enzymol. 262, 363 (1995).
18. J. A. Piccirilli, J. S. Vyle, M. H. Caruthers, T. R. Cech, Nature 361, 85 (1993).
19. H. Pelletier, M. R. Sawaya, W. Wolfle, S. H. Wilson, J. Kraut, Biochemistry 35, 12762 (1996); I. Slaby, B. Lind, A. Holmgren, Biochem. Biophys. Res. Commun. 122, 1410 (1984); G. C. King, C. T. Martin, T. T. Pham, J. E. Coleman, Biochemistry 25, 36 (1986); E. Ferrari et al., J. Virol. 73, 1649 (1999).
20. S.-Z. Yan, Z.-H. Huang, R. S. Shaw, W.-J. Tang, J. Biol. Chem. 272, 12342 (1997).
21. Y. Liu, A. E. Ruoho, V. D. Rao, J. H. Hurley, Proc. Natl. Acad. Sci. U.S.A. 94, 13414 (1997).
22. W. S. Sheldrick and E. Rieke, Acta Crystallogr. B34, 2324 (1978); K. I. Varughese, C. T. Lu, G. Kartha, J. Am. Chem. Soc. 104, 3398 (1982); N. Padmaja, S. R. Ramakumar, M. A. Viswamitra, Bull. Chem. Soc. Jpn. 64, 1359 (1991).
23. C. W. Dessauer and A. G. Gilman, J. Biol. Chem. 272, 27787 (1997).
24. W.-J. Tang, M. Stanzel, A. G. Gilman, Biochemistry 34, 14563 (1995).
25. J. J. Tesmer and S. R. Sprang, Curr. Opin. Struct. Biol. 8, 713 (1998).
26. L. S. Beese and T. A. Steitz, EMBO J. 10, 25 (1991); T. A. Steitz, Curr. Opin. Struct. Biol. 3, 31 (1993); H. Pelletier, M. R. Sawaya, A. Kumar, S. H. Wilson, J. Kraut, Science 264, 1891 (1994).
27. S. Doublié, M. R. Sawaya, T. Ellenberger, Structure 7, R31 (1999).
28. S. Doublié and T. Ellenberger, Curr. Opin. Struct. Biol. 8, 704 (1998).
29. S. G. Sarafianos, V. N. Pandey, N. Kaushik, M. J. Modak, J. Biol. Chem. 270, 19729 (1995); V. N. Pandey, N. Kaushik, M. J. Modak, ibid. 269, 13259 (1994).
30. R. K. Sunahara et al., J. Biol. Chem. 273, 16332 (1998).
31. Single-letter abbreviations for the amino acid residues are as follows: D, Asp; I, Ile; K, Lys; N, Asn; R, Arg.
32. A. G. W. Leslie, MOSFLM 5.50 for image plate data (1997).
33. S. Bailey, Acta Crystallogr. D50, 760 (1994).
34. A. T. Brünger et al., ibid. D54, 905 (1998).
35. T. A. Jones, J. Y. Zou, S. W. Cowan, M. Kjeldgaard, ibid. A47, 110 (1991).
36. We thank F. Eckstein at the Max-Planck Institute (Göttingen) for pure ATPαS-R_p; J. Collins for technical assistance; C. Brautigam for helpful discussion and for reading the manuscript; D. Coleman and the MacCHESS staff for their assistance with data collection at the Cornell High Energy Synchrotron Source (CHESS); and L. Esser for his assistance in preparing figures. R.K.S. was supported by a postdoctoral fellowship from the Medical Research Council of Canada. This work was supported by grants from the Agence Nationale de Recherche sur le SIDA (ANRS, France) to G.G.; by NIH grants DK38828 (R.A.J.), GM34497 (A.G.G.), and DK46371 (S.R.S.); by an Innovative Technology Grant from the Stony Brook Center for Biotechnology to R.A.J.; by Welch Foundation grants I-1271 (A.G.G.) and I-1229 (S.R.S.); and by the Raymond and Ellen Willie Distinguished Chair of Molecular Neuropharmacology (A.G.G.). Coordinates for the four models have been deposited in the Protein Data Bank with the codes 1CJT, 1CJU, 1CJV, and 1CJK.

26 April 1999; accepted 22 June 1999

Staphylococcus aureus Sortase, an Enzyme that Anchors Surface Proteins to the Cell Wall

Sarkis K. Mazmanian, Gwen Liu, Hung Ton-That, Olaf Schneewind*

Surface proteins of Gram-positive bacteria are linked to the bacterial cell wall by a mechanism that involves cleavage of a conserved Leu-Pro-X-Thr-Gly (LPXTG) motif and that occurs during assembly of the peptidoglycan cell wall. A *Staphylococcus aureus* mutant defective in the anchoring of surface proteins was isolated and shown to carry a mutation in the *srtA* gene. Overexpression of *srtA* increased the rate of surface protein anchoring, and homologs of *srtA* were found in other pathogenic Gram-positive bacteria. The protein specified by *srtA*, sortase, may be a useful target for the development of new antimicrobial drugs.

Hospital isolates of *Staphylococcus aureus*, *Staphylococcus epidermidis*, and *Enterococcus faecalis* have become resistant to most, if not

Department of Microbiology and Immunology, UCLA School of Medicine, University of California, 10833 Le Conte Avenue, Los Angeles, CA 90095, USA.

*To whom correspondence should be addressed. E-mail: olafs@ucla.edu

all, known therapeutic regimens (1). Many antibiotics, including penicillin and its derivatives, target the transpeptidation reaction of bacterial cell wall synthesis, which cross-links peptidoglycan strands (2). To search for other cell wall synthesis reactions that may serve as targets for antimicrobial therapy, we have focused on the anchoring of surface proteins to the peptidoglycan of Gram-positive bacteria.